

The activity of the 2004 Geminid meteor shower from global visual observations

R. Arlt^{1*} and J. Rendtel^{1,2†}

¹International Meteor Organization, PF 600118, D-14401 Potsdam, Germany

²Astrophysikalisches Institut Potsdam, An der Sternwarte 16, D-14482 Potsdam, Germany

Accepted . Received ; in original form .

ABSTRACT

A comprehensive set of 612 hours of visual meteor observations with a total of 29077 Geminid meteors detected was analysed. The shower activity is measured in terms of the Zenithal Hourly Rate (ZHR). Two peaks are found at solar longitudes $\lambda_{\odot} = 262^{\circ}16$ and $\lambda_{\odot} = 262^{\circ}23$ with $ZHR = 126 \pm 4$ and $ZHR = 134 \pm 4$, respectively. The physical quantities of the Geminid meteoroid stream are the mass index and the spatial number density of particles. We find a mass index of $s \approx 1.7$ and two peaks of spatial number density of 234 ± 36 and 220 ± 31 particles causing meteors of magnitude +6.5 and brighter in a volume of 10^9 km^3 , for the two corresponding ZHR maxima. There were 0.88 ± 0.08 and 0.98 ± 0.08 particles with masses of 1 g or more in the same volume during the two ZHR peaks. The second of the two maxima was populated by larger particles than the first one. We compare the activity and mass index profiles with recent Geminid stream modelling. The comparison may be useful to calibrate the numerical models.

Key words: meteors, meteoroids

1 INTRODUCTION

The Geminids is the densest meteoroid stream the Earth is passing annually. Its relation to the parent object (3200) Phaethon, possibly an extinct cometary nucleus, and the very short orbital period of 1.57 years cause peculiar interest in the structure and evolution of this stream.

Both, observational evidence and theoretical modelling show that the stream crossed the Earth's orbit only from the early 19th century onwards and will continue to do so for about 100 years (Hunt et al., 1985). The first unambiguous detection of the Geminids in 1862 is referred to Greg (1872). An association with meteors observed in December 1834 (Connolly & Hoffleit, 1991), prior to that established first occurrence, remains doubtful. Notes about numerous meteors and fireballs observed on 1830 December 12–13, but without a radiant position, were published by Quételet (1841, 1861).

The stream's short period orbit close to the Sun (perihelion distance 0.14 au) with encounters of the Earth and Venus has consequences for its evolution and the characteristics of the meteoroids. Model calculations give an age of the stream of a few thousand years (Jones, 1985; Williams & Wu, 1993; Ryabova, 1999). For example, the “hollow stream” model of Jones (1985) fits the observed double peak separated by $0^{\circ}8$ in solar longitude (Rendtel, 2005) with a stream age of about 6000 years.

Analyses of single Geminid returns based on world-wide visual data collected by the International Meteor Organization (IMO) yielded the above-mentioned double peak and further possible substructures (Rendtel et al., 1993; Rendtel & Arlt, 1997). Such substructures were found to exist for several returns, possibly drifting in solar longitude by $-0^{\circ}02$ per year (Rendtel, 2005). Hence the present analysis as well as those of future returns can help to find out whether this is a drift of real structures, and if so, how these structures evolve and persist. The comparison of activity profiles – of particle flux density profiles in particular – is of special interest for the calibration of theoretical stream models.

2 DATA AND REDUCTION METHOD

The full set of visual observations of the 2004 Geminid meteor shower comprises a total of 29077 Geminids recorded during 612.03 hours of effective observing time. The observers typically record the meteors without interrupting their alertness to the sky; otherwise suitable dead time is subtracted from the observing period leading to an effective time T_{eff} . If there was no dead time, T_{eff} is identical to the length of the observing interval.

The observing conditions are quantified by an evaluation of the stellar limiting magnitude (LM) for various times of the observation. This quantity describes both the quality of the sky and the perceptual capabilities of the observer. Reports without an LM are not used for this analysis.

The field of view of the observer is not restricted. **According**

* E-mail: visual@imo.net

† E-mail: jrendtel@aip.de

to Koschack & Rendtel (1990a), 1.3% of the meteors are seen outside a field of 105° diameter. The alternative of restricting the field of view by a circular frame over the observer has the advantage of a well defined observed volume in the atmosphere. However, the installation of the frame has the disadvantage of making meteor observations less mobile and less attractive to amateur astronomers thereby reducing the amount of data available enormously.

Observers are considered individual ‘detectors’. Even though several people may observe together, they neither agree upon the magnitude of a meteor nor do they ‘negotiate’ the classification of a meteor as a shower member or sporadic meteor. Even though these observers do see common meteors, their individual evaluation of the events adds to the accuracy of the average as they are independent measurements of the same quantity.

A uniform distribution of observing places on the globe would be ideal for the construction of a full activity profile of a meteor shower lasting several days. Because of the oceans this is hardly possible, but the spacing is small enough to provide an overlap of observing periods on different continents. The largest gap is between the Hawaiian Islands and Japan with a minimum distance of about 5900 km, or about 60 degrees in longitude corresponding to 4 hours time lapse. However, the radiant is above the horizon for most of the night allowing a reasonable overlap of the observing intervals.

The data allow the direct determination of two observational quantities. One is the population index r describing the exponential increase of meteor numbers towards fainter magnitudes. The variation of the population index can thus describe the particle mass distribution at various places within the meteoroid stream. The other quantity is the Zenithal Hourly Rate (ZHR) which is defined as the number of visible meteors **reduced to a limiting magnitude of LM = +6.5** and the radiant of the meteor shower is in the local zenith. The first of the two conditions requires a correction for observing conditions for each data record. This correction involves r , because an observer facing poor sky conditions misses fewer meteors when r is low than when r is high. The population index thus serves two purposes: the determination of the mass distribution in the stream and the determination of a standard activity measure such as the ZHR.

We start the analysis of a meteor shower with the determination of the temporal variation of r . **This is done** in the following Section, while the ZHR reduction is presented in Section 4. The mass index and the particle number density in space are the physical quantities of a meteoroid stream and are determined in Section 5.

3 THE POPULATION INDEX

The derivation of the population index requires the knowledge of the detection probability of a typical observer to see a meteor of a given magnitude. Since this probability depends on the limiting magnitude of the observer, it is wise to give it as a function of the difference to the limiting magnitude, Δm . These probabilities $p(\Delta m)$ were taken from Koschack & Rendtel (1990b).

In principle, meteor numbers as a function of Δm can now be fitted by an exponential function leading to the base r . This is not an optimal way of determining the population index, because the fit function has two free parameters of which we throw one away (**the intercept**). **Statistically, this is a waste of information in the data set. As a consequence, the uncertainty of r from an**

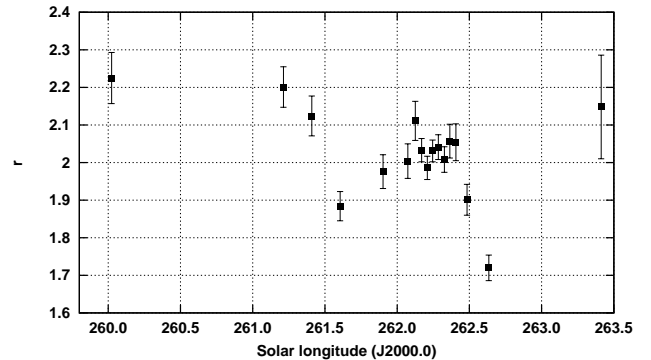


Figure 1. Population index profile of the 2004 Geminids. In the period 261° – 263° , each point represents data of 1000 and 2600 Geminids.

exponential fit is twice the uncertainty from a one-parameter relation between the magnitude distribution and r .

The approach used here applies Monte-Carlo simulations of artificial magnitude distributions $n(\Delta m)$ for a given r applying the detection probabilities $p(\Delta m)$ to the distribution. The average value $\overline{\Delta m}$ of this distribution is a monotonous function of r . A large number of simulated magnitude distributions delivers a well converged value of $\overline{\Delta m}$ for each prescribed r . An observed value of $\overline{\Delta m}$ can thus be converted into a population index r without a fit function. The resulting scatter of r -values has indeed half the value of the fit function method.

The simulated data are given by Arlt (2003) in terms of a conversion table between $\overline{\Delta m}$ and r as well as a table with the errors of r as a function of r and n , the total number of meteors involved in $\overline{\Delta m}$.

The full set of Geminid observations provides us with 3192 magnitude distributions with 24 947 shower meteors. We excluded observing periods with limiting magnitudes of $LM < 5.5$ leading to a remaining set of 2800 distributions comprising 22 198 Geminid meteors. The distribution of Geminid observations over time is far from homogeneous. For periods with few reports, magnitude distributions from a much longer time span need to be compiled in one population index than for periods with numerous reports. We apply an adaptive bin size for the population index profile. The algorithm collects magnitude distributions until data of 1000 Geminids are gathered and produces an r -value. In order to prevent the algorithm from binning in too fine steps, a minimum bin width of $0^\circ.04$ was set. This width corresponds to 56 min near the Geminid maximum night.

During the Geminid maximum, up to 2600 Geminids go into one population index. The time series of r for the 2004 Geminid meteor shower is shown in Fig. 1. Large values of r correspond to large fractions of faint meteors. The time axis is always given in terms of solar longitude referring to equinox J2000.0. Solar longitudes correspond to the actual position of the Earth in its orbit and make features easily comparable with features of other years’ Geminid returns.

Bearing in mind that the activity maximum of the Geminids is expected to occur slightly after $\lambda_\odot = 262^\circ$, we are specially interested in the features near that time. The population index is $r \sim 2$ in the maximum period of $261^\circ.8$ – $262^\circ.4$. The exception is a significant increase to $r = 2.11 \pm 0.05$ at $\lambda_\odot = 262^\circ.13$ corresponding to 2004 Dec 13, $20^{\text{h}}40^{\text{m}}$ UT. After $262^\circ.2$, a lower and nearly constant r was observed. More precisely, there is a weak tendency of an increase of r from 2.00 to 2.05 during these 5 hours.

The time after $262^{\circ}.4$ is characterized by a steep decrease of r to 1.7 during the course of about 6 hours (2004 Dec 14, $3^{\text{h}}-9^{\text{h}}$ UT. A low population index corresponds to an increased fraction of bright meteors. The end of the decrease was observed by observers in the US, but no further observations are available from the Pacific and Asian geographical longitudes, before European observations set in to deliver the population index at $\lambda_{\odot} = 263^{\circ}.4$.

4 THE ZENITHAL HOURLY RATES

The ZHR is an observational quantity as it refers to the meteor number a single observer can see under certain conditions. Its temporal variation is determined as a step toward the physical quantity of the meteoroid stream, which is the number of particles in a given volume.

The temporal ZHR profile of an individual observer is certainly not a good representation of the activity, on the one hand because subjective skills will affect the meteor rates, and on the other hand because no closed profile around the clock can be constructed. Our approach is based on the collection of a large amount of data, and the conclusions are based on the average ZHR from a wide variety of observers.

In general, the total correction factor necessary to obtain an individual ZHR is computed by

$$C_i = \frac{r^{6.5-LM} F}{T_{\text{eff}} \sin h_R} \quad (1)$$

where r is the population index derived in the previous step of data reduction, LM is the stellar limiting magnitude given by the observer, F corrects for possible field-of-view obstructions, T_{eff} is the effective observing time, and h_R is the elevation of the radiant of the meteor shower. These values refer to periods of observing time which have typical durations of 1 hour, but may be as short as 5 minutes when high meteor shower activity is experienced. Breaks and dead time for notes are accounted for in the effective time T_{eff} . Since the radiant elevation does not vary linearly with time, we use the precise average $\int_{t_1}^{t_2} \sin h_R dt / (t_2 - t_1)$ instead of the correction in (1).

The average ZHR for a specific period of time is computed with the total correction factors C_i as weights, where the index i refers to the individual observing periods with their limiting magnitude, field obstruction, effective duration and radiant elevation.

For large meteor numbers, the weighted average is then

$$\text{ZHR} = \frac{\sum_i^N n_i}{\sum_i^N C_i^{-1}}, \quad (2)$$

where N is the total number of observing periods selected for a certain determination of the ZHR and n_i are the Geminid numbers in the individual periods.

The full activity profile of the 2004 Geminids as derived by the above procedure is shown in Fig. 2. The same values are given in numerical detail in Tab. 1. The solar longitudes refer to equinox J2000.0. The error margins result from

$$\Delta\text{ZHR} = \text{ZHR} / \sqrt{\sum_i^N n_i} \quad (3)$$

being solely the 95% confidence interval of independent-event frequencies such as meteor rates. Table 1 also gives an average population index r . When each of the observing records is corrected for the limiting magnitude, r is interpolated between the values of Fig. 1. The averages of these interpolated population indices are also given in the Table.

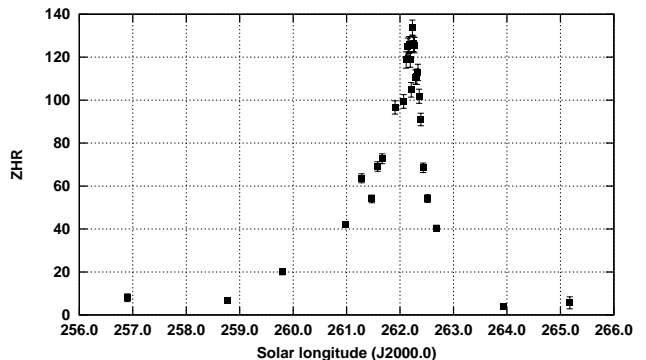


Figure 2. ZHR profile of the 2004 Geminids.

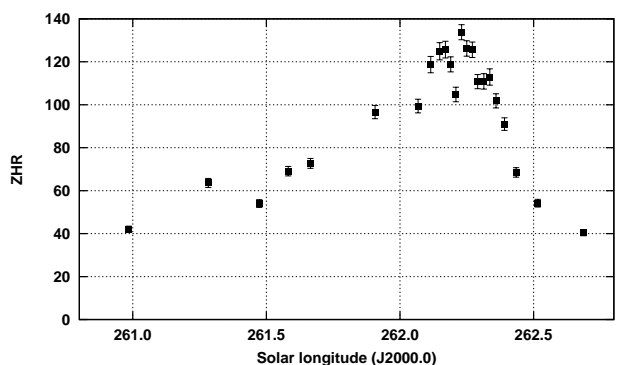


Figure 3. Magnification of the ZHR profile of the 2004 Geminids near their maximum activity.

A double maximum was found with a first peak at $\lambda_{\odot} = 262^{\circ}.16$ and a second, slightly higher peak at $\lambda_{\odot} = 262^{\circ}.23$. These solar longitudes correspond to 2004 Dec 13, $21^{\text{h}}20^{\text{m}}$ UT and $23^{\text{h}}00^{\text{m}}$ UT. The lower value of $\text{ZHR} = 104.8$ between the two peaks coincides with the low population index of $r = 1.99$ at nearly the same time. Because most of the observations have $LM < 6.5$, the correction to a ZHR is smaller if the population index is lower, and the activity dip may be entirely due to the population index variation. This may be real on its own, nevertheless, a test run recomputed a ZHR-profile with a constant $r = 2$. The resulting averages still exhibit the double maximum with $\text{ZHR} = 127 \pm 4$ and $\text{ZHR} = 129 \pm 3$ and a minimum in between with $\text{ZHR} = 109 \pm 3$. An artifact because of the uneven distribution of observation around $LM = 6.5$ can thus be excluded.

5 STREAM PARAMETERS: MASS INDEX AND PARTICLE NUMBER DENSITY

The population index r and the ZHR are observational quantities. In order to obtain physical quantities of the meteoroid stream which can be compared with other streams, we derive the distribution of particles over mass and the particle number density in space.

The exponential distribution of meteors versus magnitude converts to a power-law distribution versus meteoroid mass. The derivation of the mass index is straight-forward if there is a constant fraction of meteoroid kinetic energy being converted into luminosity. In reality this fraction depends on mass. The mass index is computed by

Table 1. ZHR activity profile of the 2004 Geminids. The number of observing records contributing to an average ZHR is N , the total number of Geminids in these records is n_{GEM} . The column LM gives the average limiting magnitude of the N observing periods contributing to an average, and r is the population index at each time. The population indices are interpolated between the values plotted in Fig. 1.

Dec	λ_{\odot}	N	n_{G}	ZHR	LM	r
8.72	256°900	4	26	8.0 ± 1.8	6.60	2.23 ± 0.07
10.56	258°776	11	79	6.9 ± 0.8	6.43	2.23 ± 0.07
11.57	259°799	13	203	20.1 ± 1.4	6.13	2.23 ± 0.07
12.74	260°984	90	968	42.1 ± 1.4	6.13	2.21 ± 0.06
13.03	261°282	76	951	63.6 ± 2.1	6.30	2.18 ± 0.05
13.22	261°473	160	938	54.0 ± 1.8	6.85	2.05 ± 0.05
13.32	261°582	124	973	69.1 ± 2.2	6.60	1.92 ± 0.04
13.40	261°665	144	957	72.7 ± 2.3	6.47	1.90 ± 0.04
13.64	261°907	134	978	96.6 ± 3.1	6.08	1.97 ± 0.05
13.80	262°067	176	942	99.4 ± 3.2	5.95	2.01 ± 0.05
13.85	262°115	160	965	118.7 ± 3.8	6.14	2.08 ± 0.05
13.88	262°148	141	954	124.9 ± 4.0	6.19	2.07 ± 0.04
13.90	262°170	146	1045	125.7 ± 3.9	6.19	2.04 ± 0.03
13.92	262°190	158	1180	118.8 ± 3.5	6.29	2.01 ± 0.03
13.94	262°209	140	967	104.8 ± 3.4	6.24	1.99 ± 0.03
13.96	262°231	164	1458	133.8 ± 3.5	6.32	2.01 ± 0.03
13.98	262°250	142	1259	126.2 ± 3.6	6.24	2.03 ± 0.03
14.00	262°271	144	1192	125.6 ± 3.6	6.25	2.04 ± 0.03
14.02	262°291	137	1119	110.8 ± 3.3	6.29	2.04 ± 0.03
14.04	262°314	121	958	110.9 ± 3.6	6.28	2.02 ± 0.03
14.06	262°336	110	863	112.9 ± 3.8	6.30	2.02 ± 0.04
14.09	262°359	133	969	101.8 ± 3.3	6.34	2.04 ± 0.04
14.12	262°391	149	955	91.0 ± 2.9	6.49	2.06 ± 0.05
14.16	262°435	174	961	68.5 ± 2.2	6.57	2.00 ± 0.05
14.24	262°515	191	922	54.2 ± 1.8	6.44	1.87 ± 0.04
14.41	262°687	207	892	40.4 ± 1.4	6.31	1.83 ± 0.06
15.63	263°926	7	28	4.1 ± 0.8	6.51	2.15 ± 0.14
16.86	265°177	1	3	5.6 ± 2.8	6.03	2.15 ± 0.14

$$s = 1 + 2.5b \log r \quad (4)$$

where $b = 0.92$ after Verniani (1973) and accounts for the above mentioned variability of the energy fraction. The mass index profile of the 2004 Geminids is shown in Fig. 4; the solar longitudes of the points of average s are the same as in the population index profile of Fig. 1. The error transmission from r to s leads to

$$\Delta s = 2.5b \log r \frac{\Delta r}{r} \quad (5)$$

These are the margins plotted in Fig. 4. The additional uncertainty in b does not enter the error bars there.

Another physical quantity of a meteoroid stream is its spatial number density of particles ρ in terms of particle numbers per unit volume. It is the same as the flux density Q which is different only by the factor of the entry velocity,

$$Q = \rho V_{\infty}. \quad (6)$$

The physical quantity which allows for a comparison between different meteoroid streams is the spatial number density though.

The observed number of meteors up to magnitude +6.5 is not complete because of the limited perception probability for faint meteors. We have to extrapolate the meteor numbers to true meteoroid numbers using the perception probabilities as a function of distance to the limiting magnitude. The extrapolation again involves r and is described in detail by Koschack & Rendtel (1990a,b). The typical observed area and the relation to an effective collection area are

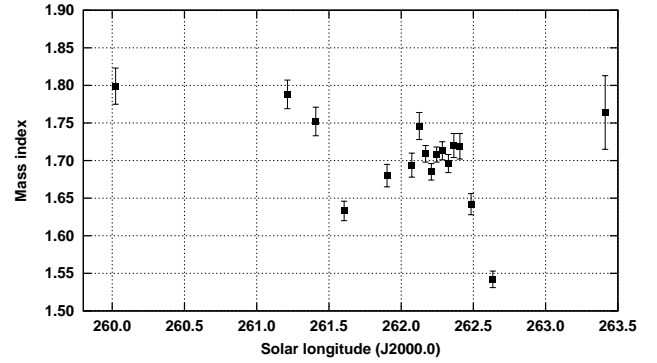


Figure 4. Mass index index profile of the 2004 Geminids.

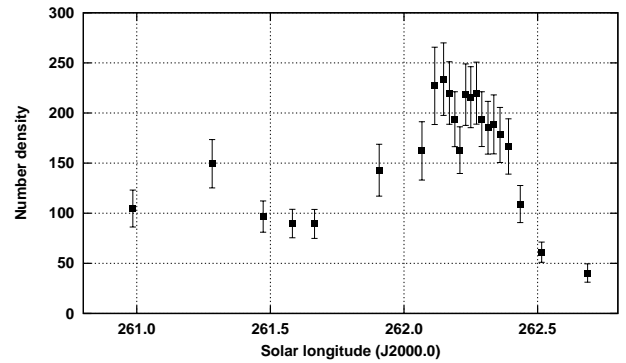


Figure 5. Spatial number density profile of the 2004 Geminids near their maximum activity. The results refer to particles causing meteors of magnitude +6.5 or brighter and are in units of particles per 10^9 km^3 .

also derived therein. The effective collecting area was derived from extensive determinations of the detection probabilities of meteors among various observers across their field of view.

The particle number density profile of the 2004 Geminids obtained by this procedure is plotted in Fig. 5 showing numbers of particles causing meteors up to magnitude +6.5. This magnitude is caused by particle masses of $4.6 \cdot 10^{-4} \text{ g}$ (cf. Verniani 1973; Hughes 1987). The unit for the number density is 10^{-9} km^{-3} , i.e. particles in a cube of 1000 km edge length. The corresponding flux density for the highest peak in Fig. 5 is $0.03 \text{ km}^{-2} \text{ h}^{-2}$. We repeat Fig. 5 in terms of flux in Fig. 6 for convenience.

When considering only particles with masses down to a cer-

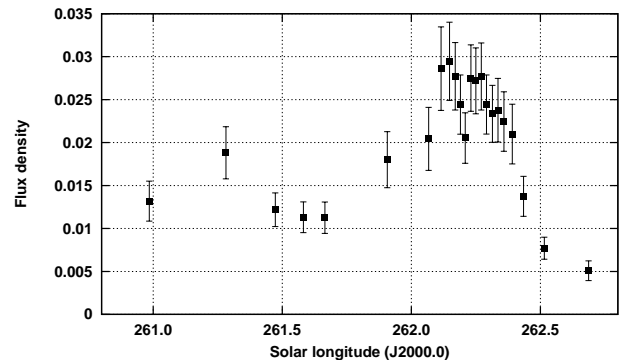


Figure 6. Repetition of Fig. 5 in terms of flux density for particles causing meteors of magnitude +6.5 or brighter. The unit of the flux is $\text{km}^{-2} \text{ h}^{-1}$.

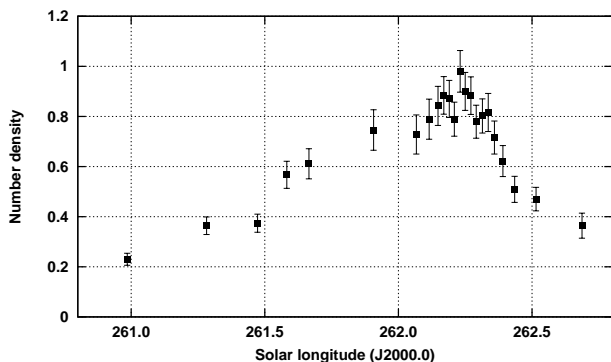


Figure 7. Spatial number density profile of the 2004 Geminids for particle masses or ≥ 1 g. The unit is again particles per 10^9 km 3 .

tain value, we can directly compare meteoroid streams. Fig. 7 shows the spatial number density of particles with masses ≥ 1 g. At the Geminids' velocity, these particles cause meteors of magnitude -1 . At maximum, there is about 1 particle in any box of 1000 km edge length. This corresponds to a flux density of about $1.4 \cdot 10^{-4}$ km $^{-2}$ h $^{-2}$. The extrapolation to the true number of meteoroids from visual observations is now much less severe whence the smaller error margins.

The highest particle number density down to a mass of $4.6 \cdot 10^{-4}$ g occurred at the first ZHR peak, whereas the highest density of only the heavier particles with ≥ 1 g coincided with the second ZHR peak. The time lapse between the two peaks is smaller for the more massive particles than for the smaller particles. It also appears that the number density profile of the larger particles is wider (full width at half maximum about $0^\circ.9$ in solar longitude) than the profile of the entire 'visual' stream (about $0^\circ.6$).

The Geminid meteoroid stream has the highest particle number density in space among the annual meteor showers. This does not manifest in an extraordinarily high ZHR because of the relatively slow geocentric velocity. The influence of the speed is twofold. First, as the Earth moves through the stream with a lower relative velocity, it collects fewer particles. Second, the amount of kinetic energy converted into meteor brightness is much lower. A Geminid meteoroid with a mass of 1 mg is 2.3 magnitudes fainter than a Perseid meteoroid of the same mass. When we observe the Geminid meteor shower, we observe ten times more massive particles than during the Perseids. This means that the particle content down to a given mass is larger for the Geminids than for the Perseids if they exhibit the same ZHR and population index r .

6 DISCUSSION

A recent analysis of data collected over 60 years (Rendtel, 2005) shows that the rate and density profiles are remarkably constant. Even the dip at $\lambda_\odot = 262^\circ.2$ which occurred in previous returns is obvious in the 2004 data shown in Fig.3. A double peak superimposed with a broad plateau-like profile lasting for about 12 hours between is a permanent feature of the stream and supports modelling results of Jones (1985) and Ryabova (2001). The latter work identifies the two activity peaks as sub-structures in the stream which are caused by particles ejected before and after perihelion passage of the parent object. A compilation of observational data by Ryabova (2001) shows that the separation of the two activity peaks decreases with meteoroid mass. We find the same effect in

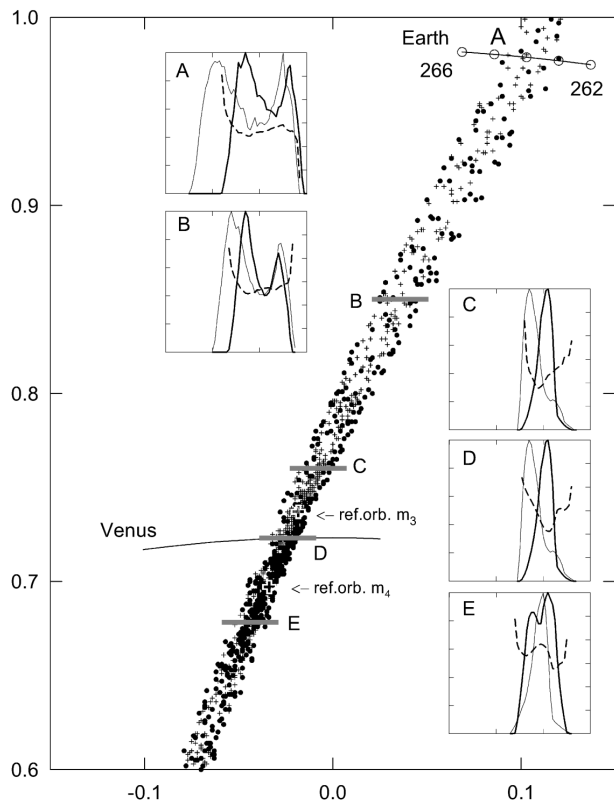


Figure 8. Various cross-sections through the Geminid meteoroid stream by courtesy of Ryabova (2004).

the 2004 Geminid data. The peaks in spatial number density for particles down to a mass of $4.6 \cdot 10^{-4}$ g are separated by $\Delta\lambda_\odot = 0^\circ.11$ in solar longitude. The peaks of particles which are more massive than 1 g are separated by only $\Delta\lambda_\odot = 0^\circ.06$ according to Fig. 7

The peak ZHR of about 130 found during the 2004 return supports the assumption of a slightly increasing activity over the last decades. Other fine structures are not visible in the 2004 data set due to the uneven distribution of observations. However, a minor peak close to $\lambda_\odot = 261^\circ.3$ coincides with peaks also found in previous data sets (Rendtel, 2005).

It has been argued that systematic errors stemming from radiant-height variations of the observable quantities may affect the results. The influence of the radiant elevation of the population index was studied by Bellot Rubio (1995). The single-body approach to the integration of the luminosity of the meteor led to a reduced population index if the radiant is not in the zenith. Observations, however, did not show a clear dependence of r on the radiant elevation. The Geminids are special among the major meteor showers in that they transit near 2 h local time, while the other major-shower radiants transit near dawn or during daytime. Observations from different geographical longitudes thus produce an entire mixture of radiant elevations in one average of r or ZHR. The influence of any possible radiant height dependence of r is averaged out in most cases. The exception is the low $r = 1.72$ at $\lambda_\odot = 262^\circ.64$ which is derived from magnitude distributions by three observers in California, Iowa, and Virginia who did not face very different radiant heights (about 8° maximum difference). The reader may be warned about that particular value of being uncertain – the finding

of a decrease of r after the Geminid maximum remains unchanged though, with the value at $\lambda_{\odot} = 262^{\circ}5$ based on 1000 Geminids.

Recent stream modelling of the Geminids was published by Ryabova (2004) based on an evolutionary mathematical model. The model provides density profiles along cross-sections through the stream. However, a calibration of the model is required in order to fix the actual path of the Earth through the Geminid stream. Flux density profiles from visual observations may provide this calibration.

The 2004 Geminids show a mass index peak just before the first of the two highest activity peaks. A plateau of the mass index follows, and the second activity peak is followed by a slight increase in the mass index. This picture matches the cross-section A of the model of Ryabova (2004) best. For direct comparison with our Figs. 4 and 6, we reproduce the relevant figure therein in Fig. 8.

Because of their abundance, visual observations are still a powerful method for the determination of the particle content and mass index of meteoroid streams.

ACKNOWLEDGEMENTS

We are grateful to all the observer who contributed to this analysis and thank Javor Kac, Slovenia, for his help with the input of observational data. We are grateful to Janko Richter, Germany, for his help on statistical issues.

REFERENCES

- Arlt R., 2003, WGN, 31, 77
 Bellot Rubio L.R., 1995, A&A 301, 602
 Connolly L.P., Hoffleit D., 1991, BAAS, 23, 941
 Greg R.P., 1872, MNRAS, 32, 345
 Hughes D.W., 1987, A&A 187, 879
 Hunt J., Williams I.P., Fox K., 1985, MNRAS, 217, 533
 Jones J., 1985, MNRASoc. 217, 523
 Koschack R., Rendtel J., 1990a, WGN, 18, 44
 Koschack R., Rendtel J., 1990b, WGN, 18, 119
 Quételet A., 1841: Nouveau catalogue des principales apparitions d'étoiles filantes. Acad. Royale de Bruxelles.
 Quételet A., 1861: Sur la physique du globe, des étoiles filantes aperçu historique. Chap. IV, Sur la physique di globe. 266–322.
 Rendtel J., 2005, EMP, in press
 Rendtel J., Arlt R., 1997, WGN, 25, 75
 Rendtel J., Arlt R., Brown P., 1993, WGN, 21, 19
 Ryabova G.O., 1999, Solar System Res., 33, 224
 Ryabova, G., 2001, Mathematical model of the Geminid meteor stream formation, Proc. Meteoroids 2001, Swedish Inst. Space Phys., Kiruna, ESA SP-495, 77–81.
 Ryabova, G.O., 2004, In: M. Triglav-Čekada, C. Trayner (eds.), Proc. Int. Meteor Conf. 2003, Int. Meteor Org., 131
 Verniani, F, 1973, J. Geophys. Res. 78, 8429
 Williams I.P., Wu Z., 1993, MNRAS, 262, 231

This paper has been typeset from a $\text{T}_{\text{E}}\text{X}/\text{L}^{\text{A}}\text{T}_{\text{E}}\text{X}$ file prepared by the author.